Nephogram super-resolution algorithm using over-complete dictionary via sparse representation

JIN Wei, FU Randi, YE Ming

Faculty of Information Science & Technology, *Ningbo University*, *Ningbo* 315211, *China*

Abstract: Motivated by the fact that image patch can be sparse represented using a suitable over-complete dictionary, a nephogram super-resolution algorithm via sparse representation using over-complete dictionary is presented. During the experiment two dictionaries $\boldsymbol{D}_{\mathrm{l}}$ and $\boldsymbol{D}_{\mathrm{h}}$ for the low-resolution and high-resolution nephogram patches were trained jointly in order to guarantee that the low-resolution and high-resolution patch pair possesses similar sparse representations as to their own dictionary. Through solving optimization problem, the sparse representation for each low-resolution nephogram patch with respect to $\boldsymbol{D}_{\mathrm{l}}$ was obtained, and the representation coefficients were applied to $\boldsymbol{D}_{\mathrm{h}}$ in order to generate the corresponding high-resolution nephogram patch. At the end of experiment the high-resolution nephogram which satisfies the reconstruction constraint was achieved by using gradient descent algorithm. Numerical experiments for infrared and visual nephogram demonstrate the effectiveness of the proposed algorithm. Moreover, the proposed algorithm outperforms interpolation based methods in terms of visual quality and the Peak Signal to Noise Ratio (PSNR).

Key words: nephogram, super-resolution, over-complete dictionary, dictionary training, sparse representation

CLC number: TP751/TP391 **Document code:** A

Citation format: Jin W, Fu R D and Ye M. 2012. Nephogram super-resolution algorithm using over-complete dictionary via sparse representation. Journal of Remote Sensing, 16(2): 275–285

1 INTRODUCTION

Clouds affect the Earth's weather system. As an important branch of remote sensing, meteorological satellite nephogram is an important tool for the weather forecast and cloud evolution. Currently, meteorological satellite can provide considerable imaging channels, but the resolutions of different channels often vary. For example, by the limitations of technical and the received radiation wavelength, the resolution of infrared channel tends to be lower, which brings an adverse impact on the integrated use of multi-channel data and also increases the difficulty of data analyzing and system designing (Georgiev & Kozinarova, 2009; Ricciardelli, et al., 2008). If down-sampling the high-resolution channel data to make it consistent with the low-resolution channel, the valuable information of high precision data is wasted. Therefore, designing corresponding super-resolution algorithms to improve the accuracy of the low-resolution channel data has a great practical significance and application meaning.

Since Harris put forward the idea of super-resolution in twentieth century 1960s, super-resolution has attracted wide attention of the academia and some effective algorithms has been proposed and applied in remote sensing image processing (Merino, et al., 2007, Li, et al., 2010). However, current super-resolution algorithms used for remote sensing images do not consider the complexity and irregularity of the texture structure of the nephogram. Such as the traditional interpolation method to enlarge the image can not increase the information in nature, and with the increase of magnification factor, there will be serious ringing or checkerboard phenomenon in the edge regions. According to the assumption of imaging model, reconstruction constraint-based algorithm can restore high resolution image from multi-frame or single-frame low-resolution images by solving the inverse problems. However, such inverse problems are severe ill-posed, it is difficult to obtain stable solution. From manifold learning theory, Chang, et al. (2004) considered that the distinct spaces of low- and high-resolution images form the similar manifolds, and proposed a super-resolution algorithm which called Neighbor Embedding (NE). NE established the mapping between the low-resolution patch and the high-resolution one via the training samples and predicted high-resolution patch as a linear combination of the low-resolution neighbor patches; however, the algorithm had disadvantages that the obtained high-resolution images often over smoothly except for the high computational complexity. In recent years, with the development of over-complete dictionary, multiscale geometric analysis etc., image sparse representation theory has aroused great concern

Received: 2010-03-03; **Accepted:** 2010-05-06

Foundation: Natural Science Foundation of Zhejiang Province (No.Y1080778, Y1111061); Nonprofit Technology Research Program of Zhejiang Province, China (No.2010C33104); Key Project of Chinese Ministry of Education (No.209155)

First author biography: JIN Wei (1969—), male, associate professor, his research interests are wavelets, remote sensing image processing, multi-scale geometric analysis, and computer vision. E-mail: jinwei@nbu.edu.cn

(Feng, et al, 2008). The theory indicates that natural images are always sparse under the suitable over-complete dictionary (Elad & Aharon, 2006; Rauhut, et al., 2008). Sparse representation model can characterize the internal structure and the prior attribute of the image, and has been widely used in image inverse problems such as denoising, deblurring, and compressed sensing etc. Motivated by the sparse representation theory and reference the idea of the NE algorithm, a nephogram super-resolution algorithm using over-complete dictionary via sparse representation was presented to implement super-resolution for the infrared and visible nephogram.

2 THE PRINCIPLES OF THE ALGORITHM

Suppose a signal $\boldsymbol{X}\in \mathrm{R}^n$ can be represented sparsely by an over-complete dictionary $\boldsymbol{D}\in \mathrm{R}^{n\times N}(N>n)$, $\boldsymbol{D}$ contains N atoms, then the signal $\boldsymbol{X}$ can be written as $\boldsymbol{X}=\boldsymbol{D}\boldsymbol{\alpha}_0$, where $\boldsymbol{\alpha}_0\in \mathrm{R}^N$ is a vector with m ($m<<N$) nonzero entries. We construct a measurement matrix $\boldsymbol{\Phi}\in \mathrm{R}^{k\times n}$ ($k<n$) to perform projection transform for $\boldsymbol{X}$ and observe measurements $\boldsymbol{Y}=\boldsymbol{\Phi}\boldsymbol{X}=\boldsymbol{\Phi}\boldsymbol{D}\boldsymbol{\alpha}_0\in \mathrm{R}^k$. Without loss of generality, we treat $\boldsymbol{X}$ as a high-resolution image (patch), while $\boldsymbol{Y}$ as its low-resolution counter part, then the problem of image super-resolution is converted to find the sparse representation coefficients $\boldsymbol{\alpha}_0$ from measurements $\boldsymbol{Y}$ and finally reconstructs the high-resolution image $\boldsymbol{X}$. Since $k<n$, image super-resolution is an underdetermined problem. According to the theory of compressed sensing (Provost & Lesage, 2009), if $\boldsymbol{\alpha}_0$ is sparse sufficiently and matrixes $\boldsymbol{\Phi}$ and $\boldsymbol{D}$ satisfy the Restricted Isometry Property (RIP), then this underdetermined problem is to be stable. This theory provides a new way to realize image super-resolution, so designing an appropriate over-complete dictionary to obtain sparse coefficients becomes a key factor.

From the idea that low- and high-resolution images form the similar manifolds (Chang, et al., 2004; Yang, et al., 2008), we assume that low- and high-resolution image patches have the same sparse representations about their corresponding over-complete dictionary. On this basis, the training samples were split into patches to form low- and high-resolution image pairs, then a coupled over-complete dictionaries $\boldsymbol{D}_\mathrm{l}$ and $\boldsymbol{D}_\mathrm{h}$ where $\boldsymbol{D}_\mathrm{l}$ for low-resolution patches, and $\boldsymbol{D}_\mathrm{h}$ for high-resolution ones were trained by using a rational training algorithm. In the processing of super-resolution, low-resolution nephogram will split into patches in the same way, then the sparse representation with respect to the low-resolution dictionary $\boldsymbol{D}_\mathrm{l}$ will be obtained and the representation coefficients will be used for the high-resolution dictionary $\boldsymbol{D}_\mathrm{h}$ directly in order to predict the corresponding high-resolution patches. Meanwhile, in order to eliminate the block effect of the reconstruction results, we adopt an overlapping split scheme, and use the gradient descent algorithm to generate the high-resolution nephogram in order to meet the reconstruction constraints.

3 JOINT TRAINING FOR OVER-COMPLETE DICTIONARY PAIR

Firstly, we split high-resolution nephogram and its corresponding low-resolution nephogram into patches, then, choose K pairs of patches to form the training samples: $T=\{X^\mathrm{h}, Y^\mathrm{l}\}$, where $X^\mathrm{h}=\{x_i\}_{i=1}^K$ represents the high-resolution nephogram patches and $Y^\mathrm{l}=\{y_i\}_{i=1}^K$ represents the corresponding low-resolution ones (or extracted features). Our goal is to acquire two dictionaries $\boldsymbol{D}_\mathrm{h}$ and $\boldsymbol{D}_\mathrm{l}$, which are trained to contain the structures of samples, and have the similar sparse representations for each patch pair x_i and y_i with the same representation coefficients. The problem can be formulated as:

$$\{\boldsymbol{D}_\mathrm{h}, \boldsymbol{\alpha}\}=\arg\min_{\boldsymbol{D}_\mathrm{h},\boldsymbol{\alpha}}\left\|\boldsymbol{X}^\mathrm{h}-\boldsymbol{D}_\mathrm{h}\cdot\boldsymbol{\alpha}\right\|_2^2+\sum_{i=1}^K\lambda_i\left\|\boldsymbol{\alpha}_i\right\|_1 \tag{1}$$

$$\{\boldsymbol{D}_\mathrm{l}, \boldsymbol{\alpha}\}=\arg\min_{\boldsymbol{D}_\mathrm{l},\boldsymbol{\alpha}}\left\|\boldsymbol{Y}^\mathrm{l}-\boldsymbol{D}_\mathrm{l}\cdot\boldsymbol{\alpha}\right\|_2^2+\sum_{i=1}^K\lambda_i\left\|\boldsymbol{\alpha}_i\right\|_1 \tag{2}$$

where $\boldsymbol{\alpha}=\{\boldsymbol{\alpha}_i\}_{i=1}^K$ represents the sparse coefficients and λ_i balances the sparse level of the coefficients and its capability to approximate original signal. In order to keep low-resolution nephogram patches have the similar representation to high-resolution ones, Eq. (1) and Eq. (2) were joint training:

$$\{\boldsymbol{D}_\mathrm{h}, \boldsymbol{D}_\mathrm{l}, \boldsymbol{\alpha}\}=\arg\min_{\boldsymbol{D}_\mathrm{h},\boldsymbol{D}_\mathrm{l},\boldsymbol{\alpha}}\frac{1}{N}\left\|\boldsymbol{X}^\mathrm{h}-\boldsymbol{D}_\mathrm{h}\cdot\boldsymbol{\alpha}\right\|_2^2+\frac{1}{M}\left\|\boldsymbol{Y}^\mathrm{l}-\boldsymbol{D}_\mathrm{l}\boldsymbol{\alpha}\right\|+\left(\frac{1}{N}+\frac{1}{M}\right)\sum_{i=1}^K\lambda_i\left\|\boldsymbol{\alpha}_i\right\|_1 \tag{3}$$

where N and M are the number of pixels of the high- and low-resolution nephogram patches, $1/N$ and $1/M$ balance the two cost Eq. (1) and Eq. (2). For the convenience, Eq. (3) can be reformulated as:

$$\{\boldsymbol{D}_\mathrm{C}, \boldsymbol{\alpha}\}=\arg\min_{\boldsymbol{D}_\mathrm{C},\boldsymbol{\alpha}}\left\|\boldsymbol{X}_\mathrm{C}-\boldsymbol{D}_\mathrm{C}\cdot\boldsymbol{\alpha}\right\|_2^2+\sum_{i=1}^K\lambda_i'\left\|\boldsymbol{\alpha}_i\right\|_1$$

$$\boldsymbol{D}_\mathrm{C}=\begin{bmatrix}\frac{1}{\sqrt{N}}\boldsymbol{D}_\mathrm{h}\\ \frac{1}{\sqrt{M}}\boldsymbol{D}_\mathrm{l}\end{bmatrix},\ \boldsymbol{X}_\mathrm{C}=\begin{bmatrix}\frac{1}{\sqrt{N}}\boldsymbol{X}^\mathrm{h}\\ \frac{1}{\sqrt{M}}\boldsymbol{Y}^\mathrm{l}\end{bmatrix},\ \lambda_i'=\left(\frac{1}{N}+\frac{1}{M}\right)\lambda_i \tag{4}$$

Now, we apply iterative methods to solve Eq. (4). First, given dictionary $\boldsymbol{D}_\mathrm{C}$, we find represent coefficients $\boldsymbol{\alpha}_i$ for each pair of training sample $\boldsymbol{X}_{\mathrm{C},i}$ to form sparse matrix $\boldsymbol{\alpha}=\{\boldsymbol{\alpha}_i\}_{i=1}^K$, then dictionary $\boldsymbol{D}_\mathrm{C}$ can be updated according to $\boldsymbol{\alpha}$. The specific steps described as follow:

Step 1 Initialize $\boldsymbol{D}_\mathrm{C}$ with a Gaussian random matrix;

Step 2 Fix $\boldsymbol{D}_\mathrm{C}$, solving $\boldsymbol{\alpha}$ according to:

$$\boldsymbol{\alpha}_i=\arg\min_{\boldsymbol{\alpha}_i}\left\|\boldsymbol{X}_{\mathrm{C},i}-\boldsymbol{D}_\mathrm{C}\cdot\boldsymbol{\alpha}_i\right\|_2^2+\lambda_i'\left\|\boldsymbol{\alpha}_i\right\|_1 \tag{5}$$

In this step, we try to find representation coefficients for each training sample under fixed dictionary $\boldsymbol{D}_\mathrm{C}$; Eq. (5) is a L_1-norm optimization problems, which can be solved by the algorithms such as Basis Pursuit (BP), Iterative Shrinkage/ Threshold (IST), etc. (Donoho, 2006; Bioucas-dias & Figueiredo, 2007).

Step 3 Fix $\boldsymbol{\alpha}$, update $\boldsymbol{D}_\mathrm{C}$; in this step, as the sparse representation coefficient $\boldsymbol{\alpha}_i$ is known, we can ignore the second item of the right side of Eq. (4). That is:

$$\boldsymbol{D}_\mathrm{C}=\arg\min_{\boldsymbol{D}_\mathrm{C}}\left\|\boldsymbol{X}_\mathrm{C}-\boldsymbol{D}_\mathrm{C}\cdot\boldsymbol{\alpha}\right\|_2^2 \tag{6}$$

The above is a quadratic programming problem and we use the algorithm proposed by Lee(Lee, et al.,2007) to solve it;

Step 4 Iterate between **Step 2** and **3**.

After iterations (in our implementation, the number of iterations is set as 25), we can get the solution of Eq. (4) and therefore obtain the expected over-complete dictionary pair $\{\boldsymbol{D}_\mathrm{h}, \boldsymbol{D}_\mathrm{l}\}$.

4 NEPHOGRAM SUPER-RESOLUTION VIA SPARSE REPRESENTATION

In this section, we will discuss the super-resolution processing by applying the obtained dictionary pair $\{\boldsymbol{D}_\mathrm{h}, \boldsymbol{D}_\mathrm{l}\}$ to the nepho-

grams. At first, we split low-resolution nephogram into patches, then for each low-resolution patch, consider optimization problems as follow:

$$\boldsymbol{\alpha}_i = \arg\min_{\alpha_i} \left\| F\cdot \boldsymbol{D}_1\cdot \boldsymbol{\alpha}_i - F\cdot \boldsymbol{y}_i \right\|_2^2 + \lambda_i \left\| \boldsymbol{\alpha}_i \right\|_1 \tag{7}$$

where $\boldsymbol{F}$ is an operator for feature extraction, the first item of the right side Eq. (7) measures the overall similarity between reconstructed and original nephogram, while the second part is the constraint of sparsely.

We can get representation coefficients $\boldsymbol{\alpha}_i$ of each low-resolution nephogram patches by solving Eq. (7). After applying $\boldsymbol{\alpha}_i$ to $\boldsymbol{D}_\mathrm{h}$, we can obtain corresponding high-resolution nephogram patches by $\boldsymbol{x}_i=\boldsymbol{D}_\mathrm{h}\boldsymbol{\alpha}_i$. However, if we solve each local patch individually, the blocking effect would be introduced in the reconstructed high-resolution nephogram. To minimize this negative effect, an overlap blocking scheme has been adopted in this paper. Finally, gradient descent algorithm was adopted to maintain that the reconstructed high-resolution nephogram patches satisfy reconstruction constraint.

Step 1 For the low-resolution nephogram, we design an overlap block scheme: for each 3×3 patch $\boldsymbol{y}_i$, we set 1 pixel overlap in each direction such as the neighboring blocks overlap one row or column with 3 pixels overlapped. (If the magnification factor is 2×2, then the size of corresponding high-resolution patch $\boldsymbol{x}_i$ is 6×6 and 2 pixels overlap in each direction with 12 pixels overlapped between neighboring blocks; similarly, 3 pixels overlap in each direction for 3×3 amplification.)

Step 2 The patches are processed in raster-scan order in the nephogram, from left to right and top to bottom. The sparse representation coefficients $\boldsymbol{\alpha}_i$ of the nephogram patch were obtained by joint solving the following optimization problems:

$$\boldsymbol{\alpha}_i = \arg\min_{\alpha_i} \left\| F\cdot \boldsymbol{D}_1\cdot \boldsymbol{\alpha}_i - F\cdot \boldsymbol{y}_i \right\|_2^2 + \lambda \left\| \boldsymbol{\alpha}_i \right\|_1 \tag{8}$$

$$\boldsymbol{\alpha}_i = \arg\min_{\alpha_i} \left\| O\cdot \boldsymbol{D}_\mathrm{h}\cdot \boldsymbol{\alpha}_i - \boldsymbol{R} \right\|_2^2 + \beta \left\| \boldsymbol{\alpha}_i \right\|_1 \tag{9}$$

where the operator $\boldsymbol{O}$ extracts the region of overlap, $\boldsymbol{R}$ is a matrix which contains the overlap pixels of the current target patch and previously reconstructed neighboring high-resolution patch. For simplicity, we set the Lagrange multipliers λ and β to 1. Then Eq. (8) and Eq. (9) can be rewritten as:

$$\boldsymbol{\alpha}_i = \arg\min_{\alpha_i} \left\| \boldsymbol{D}'\cdot \boldsymbol{\alpha}_i - \boldsymbol{y}' \right\|_2^2 + \left\| \boldsymbol{\alpha}_i \right\|_1 \tag{10}$$

where $\boldsymbol{D}' = \begin{bmatrix} F\cdot \boldsymbol{D}_1 \\ O\cdot \boldsymbol{D}_\mathrm{h} \end{bmatrix}$, $\boldsymbol{y}' = \begin{bmatrix} F\cdot \boldsymbol{y} \\ \boldsymbol{R} \end{bmatrix}$;

Step 3 Generate the corresponding high-resolution nephogram patches $\boldsymbol{x}_i=\boldsymbol{D}_\mathrm{h}\boldsymbol{\alpha}_i$;

Step 4 After all the patches were processed, we constitute the preliminary high-resolution nephagram: $\boldsymbol{X}_0=\{x_i\}_{i=1}^K$;

Step 5 For $\boldsymbol{X}_0$, solving the following optimization problem to find the final high-resolution nehpogram which satisfies the reconstruction constraint:

$$\boldsymbol{X} = \arg_{\boldsymbol{X}}\min \left\| \boldsymbol{S}\cdot \boldsymbol{B}\cdot \boldsymbol{X} - \boldsymbol{Y} \right\|_2^2 + \left\| \boldsymbol{X} - \boldsymbol{X}_0 \right\|_2^2 \tag{11}$$

where $\boldsymbol{B}$ represents a blurring filter of nehpogram (Considering that the low-pass filter of nephogram is mainly caused by atmospheric turbulence, whose transfer function can be approximately expressed as $B(u,v)=\exp[-c(u^2+v^2)^{5/6}]$, in this paper set $c=0.00025$), and $\boldsymbol{S}$ is the down-sampling operator. The first item of right side of Eq. (11) represents the degradation model of nehpogram, and the second item describes the similarity between reconstructed nehpogram and ideal nehpogram. Solving Eq. (11) using gradient descent algorithm, we can get desired super-resolution nephogram $\boldsymbol{X}$.

5 NUMERICAL EXPERIMENTS

In this section, numerical experiments were performed to demonstrate the effectiveness of the proposed Super-resolution (SR) algorithm. In our experiments the proposed algorithm was compared with Neighborhood Embedding (NE) algorithm (Chang, 2004) (set neighborhood parameters k=10), Nearest Neighbor Interpolation algorithm, and Bi-cubic Interpolation algorithm. The performances of different SR algorithms were evaluated in terms of visual quality, PSNR and Entropy.

The training nephograms were selected from the high-resolution channel (visible channel) of MTSAT satellite. First, we selected a set of original visible nephograms to generate corresponding low-resolution nephograms by blurring and down-sampling. Then, the high- and low-resolution nephograms were split into patches to form training samples by the method we described in section 3. In this experiment, we select 10000 nephogram patch pairs to train two dictionaries $\boldsymbol{D}_\mathrm{l}$ and $\boldsymbol{D}_\mathrm{h}$, both of which contain 1024 atoms. (This dictionary pair can be used to implement 2×2 magnification, and in order to change the magnification factor, simply re-training the appropriate dictionary pair). In the implementation of the specific algorithm, we also selected an appropriate operator to extract features of the low-resolution patch. As for nephogram super-resolution, the high frequency components of the low-resolution nephogram contained more useful information than the low frequency components, we adopt Chang's method (Chang, 2004), which selected the first-order template [–1, 0, 1] and second-order template [1, 0, –2, 0, 1] as feature extraction operators for Eq. (7) and Eq. (8).

We applied the trained over-complete dictionaries to the visible and infrared nephogram super-resolution. The test nephograms were collected form the infrared 2(IR2) and visible channel of MTSAT satellite at 12:06 on august 62009, when Typhoon Morakot had generated. In order to analyze the results easily, we cut out a specific area from the original nephogram and ensure that the selected area contained complete typhoon cloud relatively. As for the visible nephogram which were higher resolution originally, we design a simulation experiment. First, the original visible nephogram was degraded according to the degradation model to generate corresponding low-resolution nephogram, then magnify it to implement super-resolution, and finally we evaluated the performance of the algorithms in terms of Peak Signal to PSNR and Entropy. As for the infrared nephogram, due to its original low-resolution, we apply super-resolution to it directly and evaluate the results of various algorithms in terms of Entropy merely. Fig. 1 illustrates the simulation results on the visible nephogram with magnification factor 2×2 using various methods.

The experiment results show that the algorithms based on interpolation can have a better performance in magnifying large-scale structure in the nephogram. However, the textures with small-scale were lost significantly. It is clear from the zoom in regions that the results of algorithms based on interpolation exists serious checkerboard effect and the overall image looks blurry. The NE algorithm is similar to ours in the sense that both algorithms can keep small-

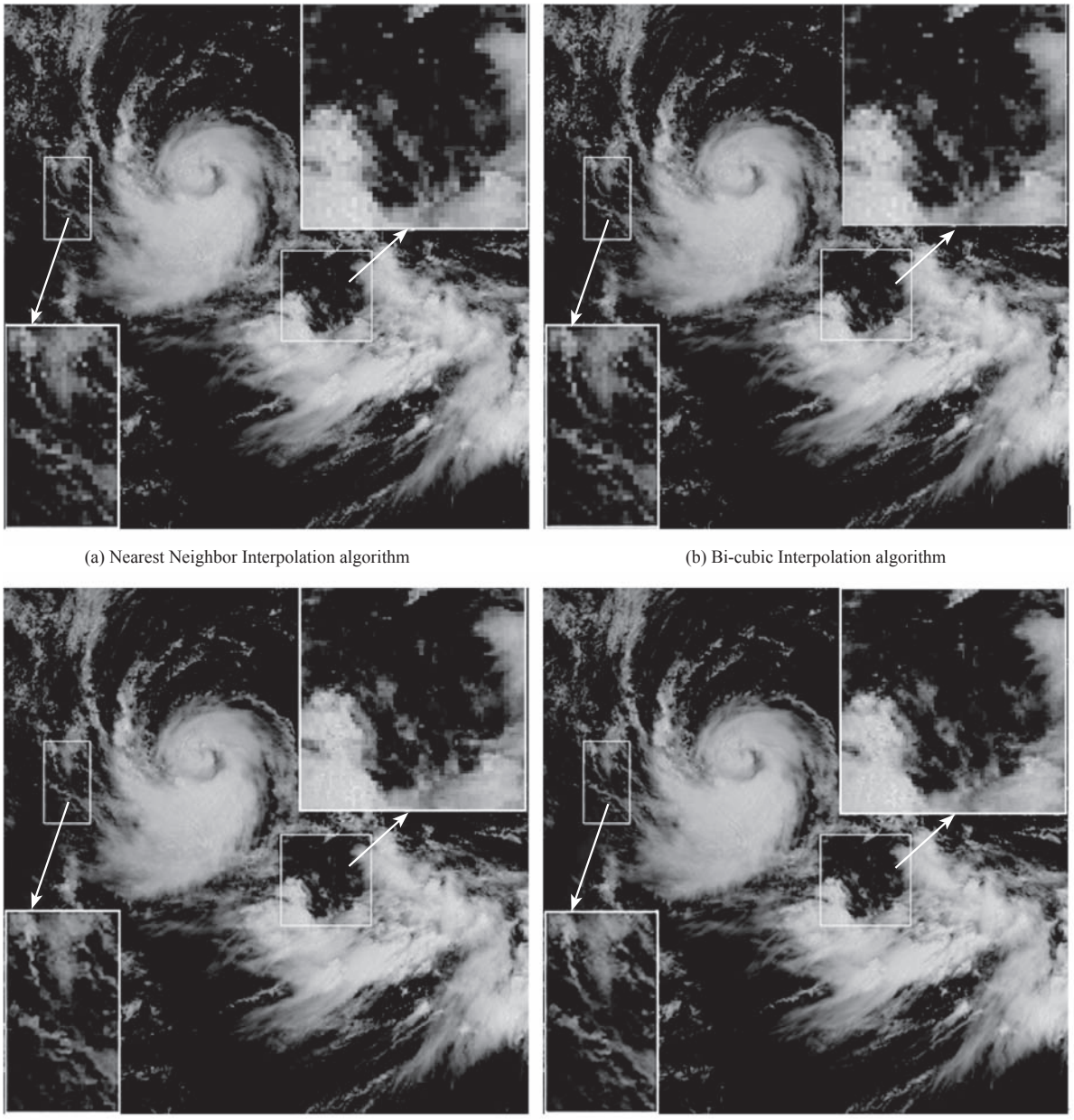

(a) Nearest Neighbor Interpolation algorithm

(b) Bi-cubic Interpolation algorithm

(c) Neighborhood embedding algorithm

(d) Proposed algorithm

Fig. 1 The super-resolution reconstruction images using various algorithms

scale details such as texture efficiently, but the proposed algorithm has a clearer reconstruction result. Moreover, NE algorithm's reconstruction result depends on the number of neighborhood. On the other hand, NE algorithm is more complex (when algorithms run in a notebook with core 1.83 G CPU, 1 MB RAM, NE algorithm takes 93.51 s while the proposed algorithm takes 37.26 s). Therefore, the proposed algorithm is relatively faster.

In order to evaluate the performance of various algorithm quantitatively, PSNR and Entropy were used as objective indicator to measure the quality of reconstruction results. As for the super-resolution of nephogram, PSNR can measure the fidelity of the super-resolution results with respect to the original high-resolution nephogram, while Entropy measures the amount of information contained in the nephograms. In general, larger values indicate better quality of super-resolution results. Meanwhile, in order to test the feasibility and effectiveness of the proposed algorithm for other satellite data, we also selected the FY/2D satellite's data from IR2 and visible channel at 12:30 on March 25, 2011 in China's land area to conduct super-resolution experiments. The quantified indicators PSNR and Entropy for the super-resolution results of MTSAT and FY/2D satellites' data were listed in Table 1 (As we apply super-resolution for infrared nephograms directly, we only evaluate the performance of the various algorithms in terms of Entropy).

As can be seen from the Table, the proposed algorithm outperforms interpolation based algorithms in various evaluation indicators, both for visible and infrared nephograms. The nearest neighbor interpolation algorithm has the lowest PSNR and Entropy. As for the NE algorithm, the PSNR is similarly to our algorithm but

Table 1 Comparison of PSNR (dB) and Entropy for the reconstruction results using various algorithms

Satellite data	Various algorithms	Visible nephogram		Infrared nephogram (IR2)	
		PSNR	Entropy	PSNR	Entropy
MTSAT	Proposed algorithm	32.6693	7.5127	—	7.2304
	Neighborhood embedding	32.6704	7.2119	—	7.1291
	Nearest neighbor interpolation	27.0065	6.9364	—	7.0338
	Bi-cubic interpolation	28.4253	7.0142	—	7.0556
FY/2D	Proposed algorithm	35.8905	7.2872	—	6.9230
	Neighborhood embedding	35.2735	7.2145	—	6.8745
	Nearest neighbor interpolation	29.1769	7.0524	—	6.5237
	Bi-cubic interpolation	31.2348	7.0891	—	6.6381

in terms of Entropy, the NE algorithm is relatively poor. This also confirms that the results of NE algorithm are too smooth that some details of nephograms were lost. As the reasons for this phenomenon, we suggest that the nephograms contain rich of texture details, and the over-complete dictionary we trained can be well expressed this texture characteristics of nephograms, just appropriate for handling such signals.

6 CONCLUSIONS

This paper introduced the over-complete dictionary based sparse representation theory into nephogram super-resolution. First, the over-complete dictionary pairs which contain the information of high- and low-resolution nephogram were obtained via learning, and the overlapped blocking scheme was adopted to get sparse representation of the low-resolution nephogram respect to the low-resolution dictionary. Then the representation coefficients were applied to the corresponding high-resolution dictionary to reconstruct high resolution nephogram. The experiments results demonstrate that the proposed algorithm is better than traditional methods in terms of visual quality and quantitative indicators. It both shows the feasible and effectiveness of super-resolution for the nephogram and extends the application of the image sparse representation theory. Moreover, this paper provides a good foundation for the subsequent researches such as cloud type classification and convective cloud identification.

Acknowledgements: The authors wish to thank the anonymous reviewers for their helpful comments, which led to a significant improvement in the paper. The authors also thank Prof. Zhou Ya-xun for constructive suggestions.

REFERENCES

Bioucas-Dias J M and Figueiredo M A T. 2007. A new TwIST: two-step iterative shrinkage/thresholding algorithms for image restoration. IEEE Transactions on Image Processing, 16(12): 2992–3004

Chang H, Yeung D Y and Xiong Y M. 2004. Super-resolution through neighbor embedding. IEEE Conference on Computer Vision and Pattern Classification (CVPR), 1: 275–282

Donoho D L. 2006. For most large underdetermined systems of equations, the minimal norm near-solution approximates the sparsest near-solution. Communications on Pure and Applied Mathematics, 59(7): 907–934

Elad M and Aharon M. 2006. Image denoising via sparse and redundant representations over learned dictionaries. IEEE Transactions on Image Processing, 15(12): 3736–3745

Feng P, Wei B, Pan Y J anf Mi D L. 2008. Analysis of frequency aliasing of contourlet transform based on laplace pyramidal transform. Acta Optica Sinica, 28(11): 2090–2096

Georgiev C G and Kozinarova G. 2009. Usefulness of satellite water vapour imagery in forecasting strong convection: a flash-flood case study. Atmospheric Research, 93(1-3): 295–303

Lee H, Battle A, Raina R and Ng A Y. 2007. Efficient sparse coding algorithms In Advances in Neural Information Processing Systems (NIPS): 801–808

Li F, Jia X P, Fraser D and Lambert A.2010. Super resolution for remote sensing images based on a universal Hidden Markov Tree model. IEEE Transactions on Geoscience and Remote Sensing, 48(3):1270–1278

Merino M T, Nunez J. 2007. Super-resolution of remotely sensed images with variable-pixel linear reconstruction. IEEE Transactions on Geoscience and Remote Sensing, 45(5): 1446–1457

Provost J and Lesage F. 2009. The application of compressed sensing for photo-acoustic tomography. IEEE Transactions on Medical Imaging, 28(4): 585–594

Rauhut H, Schnass K and Vandergheynst P. 2008. Compressed sensing and redundant dictionaries. IEEE Transactions on Information Theory, 54(5): 2210–2219

Ricciardelli E, Romano F and Cuomo V. 2008. Physical and statistical approaches for cloud identification using Meteosat Second Generation-Spinning Enhanced Visible and Infrared Imager Data. Remote Sensing of Environment, 112(6): 2741–2760

Yang J C, Wright J, Huang T and Ma Y. 2008. Image super-resolution as sparse representation of raw image patches. IEEE Conference on Computer Vision and Pattern Classification (CVPR): 1–8

过完备字典稀疏表示的云图超分辨率算法

金炜，符冉迪，叶明

宁波大学 信息科学与工程学院，浙江 宁波 315211

摘 要：提出一种基于过完备字典稀疏表示的云图超分辨率算法。首先，联合训练针对低分辨率与高分辨率云图块的两个字典$\boldsymbol{D}_{\mathrm{l}}$和$\boldsymbol{D}_{\mathrm{h}}$，保证对应的低分辨率与高分辨率云图块关于各自的字典具有相似的稀疏表示；其次，通过求解优化问题，获得待处理云图每个低分辨率云图块关于$\boldsymbol{D}_{\mathrm{l}}$的稀疏表示，并将表示系数用于$\boldsymbol{D}_{\mathrm{h}}$以生成对应的高分辨率云图块；最后，运用最速下降算法，得到满足重构约束的高分辨率云图。红外与可见光云图的数值实验验证了本文算法的有效性，表明本文算法在视觉效果及PSNR指标上均优于插值方法。

关键词：云图，超分辨率，过完备字典，字典训练，稀疏表示

中图分类号：TP751/TP391 **文献标志码**：A

引用格式：金炜，符冉迪，叶明. 2012. 过完备字典稀疏表示的云图超分辨率算法. 遥感学报，16(2): 275–285
Jin W, Fu R D and Ye M. 2012. Nephogram super-resolution algorithm using over-complete dictionary via sparse representation. Journal of Remote Sensing, 16(2): 275–285

1 引 言

云是影响地球天气系统的因素之一，作为遥感技术的重要分支，气象卫星云图是预测天气变化及检测云演变过程的重要工具。目前，气象卫星虽能提供相当多的成像通道，但不同通道数据的分辨率往往不同，比如由于受接收辐射的波长和技术水平的限制，红外通道数据的分辨率往往较低，这对综合使用多通道数据进行分析不利，也会增加分析设计的难度(Georgiev和Kozinarova，2009；Ricciardelli 等，2008)；如果对高分辨率通道的数据进行抽样，使其与低分辨率通道的数据一致，则对宝贵的高精度数据信息是一种浪费。因此，设计相应的超分辨率算法，使得低分辨率通道数据的精度得以提升就有着极大的现实意义和应用价值。

自20世纪60年代Harris提出超分辨率思想以来，超分辨率技术得到了学术界的广泛重视，出现了一些行之有效的算法，并在遥感图像处理中得到了应用(Merino 等，2007；Li 等，2010)。然而，目前的遥感图像超分辨率算法大都未考虑卫星云图纹理结构的复杂性及不规则性，仅适用于特定的成像模型。如传统的插值放大算法本质上并不能增加图像的有效信息，且随着放大倍数的增加在图像的边缘区域会出现严重的振铃或棋盘现象；基于重构约束的算法则根据假设的成像模型，通过多帧或单帧低分辨率图像的逆向求解，复原出高分辨率图像，但由于此类反问题严重的病态性，往往不易得到稳定的结果；Chang 等从流形学习理论出发，认为低分辨率图像空间与高分辨率图像空间具有相似的流形，提出一种称为邻域嵌入NE(Neighbor Embedding)的超分辨率算法(Chang 等，2004)，该算法通过训练样本建立低分率图像块与高分辨率图像块的映射关系，并根据相邻低分辨率图像块的线性组合来预测对应的高分辨率图像块，但该算法计算复杂性较高，且所得的高分辨率图像往往过于平滑。

近年来，以过完备字典、多尺度几何分析等为代表的图像稀疏表示理论引起了人们的极大关注(冯鹏 等，2008)，该理论认为自然图像在合适的过

收稿日期：2010-03-03；**修订日期**：2010-05-06

基金项目：浙江省自然科学基金(编号: Y1080778，Y1111061)；浙江省公益性技术应用研究计划(编号: 2010C33104)；国家教育部科学技术研究重点项目(编号: 209155)

第一作者简介：金炜(1969—)，男，博士，副教授，主要研究方向为小波分析、遥感图像处理、多尺度几何分析以及计算机视觉。E-mail: jinwei@nbu.edu.cn。

完备字典下总存在稀疏表示(Elad和Aharon，2006；Rauhut 等，2008)。图像稀疏表示模型能够刻画图像的内在结构和先验属性，在图像去噪、去模糊、压缩感知等反问题中得到了广泛的应用；受稀疏表示理论的启发，本文借鉴NE算法的思想，提出了一种基于过完备字典稀疏表示的云图超分辨率算法，并针对红外与可见光云图进行了数值实验。实验结果不仅验证了本文算法的有效性，而且与传统的插值方法相比，本文的超分辨率算法能够更好地重构云图的纹理、轮廓等几何结构，使放大后图像具有更高的峰值信噪比。

2 算法基本原理

设具有N个原子项的过完备字典$\boldsymbol{D}\in \mathrm{R}^{n\times N}(N>n)$可稀疏表示信号$\boldsymbol{X}\in \mathrm{R}^{n}$，即$\boldsymbol{X}=\boldsymbol{D}\boldsymbol{\alpha}_0$，其中系数$\boldsymbol{\alpha}_0\in \mathrm{R}^{N}$仅包含$m$个非零项($m\ll N$)，可以构造测量矩阵$\boldsymbol{\Phi}\in \mathrm{R}^{k\times n}$($k<n$)，对$\boldsymbol{X}=\boldsymbol{D}\boldsymbol{\alpha}_0$进行投影变换，得到测量值$\boldsymbol{Y}\in \mathrm{R}^{k}$，即$\boldsymbol{Y}=\boldsymbol{\Phi}\boldsymbol{X}=\boldsymbol{\Phi}\boldsymbol{D}\boldsymbol{\alpha}_0$；不失一般性，可将$\boldsymbol{X}$看成是高分辨率图像(或图像块)，$\boldsymbol{Y}$为对应的低分辨率图像(或图像块)，则图像超分辨率问题就转化为通过测量值$\boldsymbol{Y}$寻求稀疏表示系数$\boldsymbol{\alpha}_0$，进而重构出高分辨率图像$\boldsymbol{X}$。由于$k<n$，该问题是一个欠定问题，根据压缩感知理论(Provost和Lesage，2009)，如果$\boldsymbol{\alpha}_0$足够稀疏，且$\boldsymbol{\Phi}$和$\boldsymbol{D}$满足有限等容性，则该欠定问题就存在稳定解，这就为图像超分辨率处理提供了一种新思路，而设计合适的过完备字典并求得稀疏表示系数就成为问题的关键。

本文借鉴Chang所提出的低分辨率图像空间与高分辨率图像空间具有相似流形的思想(Chang 等，2004；Yang 等，2008)，假定低分辨率与高分辨率云图块关于各自的过完备字典具有相似的稀疏表示，通过将训练样本分块，建立成对的低分辨率与高分辨率样本云图块，采用合理的过完备字典联合训练算法，训练出一对过完备字典$\boldsymbol{D}_{\mathrm{l}}$和$\boldsymbol{D}_{\mathrm{h}}$，其中$\boldsymbol{D}_{\mathrm{h}}$用于稀疏表示高分辨率云图块，$\boldsymbol{D}_{\mathrm{l}}$用于稀疏表示低分辨率云图块。在实际超分辨率处理中，将低分辨率云图以同样的方法分块，求解待处理云图的各低分辨率云图块在字典$\boldsymbol{D}_{\mathrm{l}}$上的稀疏表示，并将低分辨率云图块关于$\boldsymbol{D}_{\mathrm{l}}$的稀疏表示系数直接作用于$\boldsymbol{D}_{\mathrm{h}}$，从而预测出对应的高分辨率云图块；同时，为了消除重构云图的块效应，本文采用一种部分交叠的分块方案，并运用最速下降法，得到满足重构约束的高分辨率云图。

3 过完备字典对的联合训练

首先，将用于训练的高分辨率与对应的低分辨率云图分块，从中选取K对子云图块，组成训练样本对：$T=\{X^{\mathrm{h}}, Y^{\mathrm{l}}\}$，其中$X^{\mathrm{h}}=\{x_i\}_{i=1}^{K}$为高分辨率云图块，$Y^{\mathrm{l}}=\{y_i\}_{i=1}^{K}$为对应的低分辨率云图块(或提取的特征)；目标是训练出一对包含样本结构的字典$\boldsymbol{D}_{\mathrm{h}}$和$\boldsymbol{D}_{\mathrm{l}}$，使得$x_i$和$y_i$在$\boldsymbol{D}_{\mathrm{h}}$和$\boldsymbol{D}_{\mathrm{l}}$上具有相同的稀疏表示，而且$x_i$和$y_i$具有相同的表示系数，即：

$$\{\boldsymbol{D}_{\mathrm{h}},\boldsymbol{\alpha}\}=\arg\min_{\boldsymbol{D}_{\mathrm{h}},\boldsymbol{\alpha}}\left\|\boldsymbol{X}^{\mathrm{h}}-\boldsymbol{D}_{\mathrm{h}}\cdot\boldsymbol{\alpha}\right\|_2^2+\sum_{i=1}^{K}\lambda_i\left\|\boldsymbol{\alpha}_i\right\|_1 \quad (1)$$

$$\{\boldsymbol{D}_{\mathrm{l}},\boldsymbol{\alpha}\}=\arg\min_{\boldsymbol{D}_{\mathrm{l}},\boldsymbol{\alpha}}\left\|\boldsymbol{Y}^{\mathrm{l}}-\boldsymbol{D}_{\mathrm{l}}\cdot\boldsymbol{\alpha}\right\|_2^2+\sum_{i=1}^{K}\lambda_i\left\|\boldsymbol{\alpha}_i\right\|_1 \quad (2)$$

式中，$\boldsymbol{\alpha}=\{\boldsymbol{\alpha}_i\}_{i=1}^{K}$为稀疏表示系数矩阵，$\lambda_i$用于平衡系数的稀疏性及其对原始信号的逼近能力。为了使低分辨率云图块与对应的高分辨率云图块关于各自的字典具有相同的稀疏表示，对式(1)、式(2)联合训练：

$$\{\boldsymbol{D}_{\mathrm{h}},\boldsymbol{D}_{\mathrm{l}},\boldsymbol{\alpha}\}=\arg\min_{\boldsymbol{D}_{\mathrm{h}},\boldsymbol{D}_{\mathrm{l}},\boldsymbol{\alpha}}\frac{1}{N}\left\|\boldsymbol{X}^{\mathrm{h}}-\boldsymbol{D}_{\mathrm{h}}\cdot\boldsymbol{\alpha}\right\|_2^2+\frac{1}{M}\left\|\boldsymbol{Y}^{\mathrm{l}}-\boldsymbol{D}_{\mathrm{l}}\boldsymbol{\alpha}\right\|+\left(\frac{1}{N}+\frac{1}{M}\right)\sum_{i=1}^{K}\lambda_i\left\|\boldsymbol{\alpha}_i\right\|_1 \quad (3)$$

式中，N和M分别为高分辨率云图块与低分辨率云图块的像元，$1/N$，$1/M$可用于平衡代价函数式(1)和式(2)，为方便求解，将式(3)写成：

$$\{\boldsymbol{D}_{\mathrm{C}},\boldsymbol{\alpha}\}=\arg\min_{\boldsymbol{D}_{\mathrm{C}},\boldsymbol{\alpha}}\left\|\boldsymbol{X}_{\mathrm{C}}-\boldsymbol{D}_{\mathrm{C}}\cdot\boldsymbol{\alpha}\right\|_2^2+\sum_{i=1}^{K}\lambda_i'\left\|\boldsymbol{\alpha}_i\right\|_1$$

$$\boldsymbol{D}_{\mathrm{C}}=\begin{bmatrix}\frac{1}{\sqrt{N}}\boldsymbol{D}_{\mathrm{h}}\\ \frac{1}{\sqrt{M}}\boldsymbol{D}_{\mathrm{l}}\end{bmatrix},\ \boldsymbol{X}_{\mathrm{C}}=\begin{bmatrix}\frac{1}{\sqrt{N}}\boldsymbol{X}^{\mathrm{h}}\\ \frac{1}{\sqrt{M}}\boldsymbol{Y}^{\mathrm{l}}\end{bmatrix},\ \lambda_i'=\left(\frac{1}{N}+\frac{1}{M}\right)\lambda_i \quad (4)$$

式(4)可采用迭代的方法求解，首先给定字典$\boldsymbol{D}_{\mathrm{C}}$，求解每对训练样本$X_{\mathrm{c},i}$在$\boldsymbol{D}_{\mathrm{C}}$上的稀疏表示$\boldsymbol{\alpha}_i$，得到稀疏表示矩阵$\boldsymbol{\alpha}=\{\boldsymbol{\alpha}_i\}_{i=1}^{K}$；然后根据α更新字典$\boldsymbol{D}_{\mathrm{C}}$，具体步骤如下：

步骤 1 采用高斯随机矩阵初始化$\boldsymbol{D}_{\mathrm{C}}$；

步骤 2 固定字典$\boldsymbol{D}_{\mathrm{C}}$，求α；在这一阶段，假设字典$\boldsymbol{D}_{\mathrm{C}}$是固定的，求解各训练样本在$\boldsymbol{D}_{\mathrm{C}}$上的表示系数，即：

$$\boldsymbol{\alpha}_i=\arg\min_{\boldsymbol{\alpha}_i}\left\|\boldsymbol{X}_{\mathrm{C},i}-\boldsymbol{D}_{\mathrm{C}}\cdot\boldsymbol{\alpha}_i\right\|_2^2+\lambda_i'\left\|\boldsymbol{\alpha}_i\right\|_1 \quad (5)$$

上式为L_1优化问题，可采用基追踪、迭代收缩等算法求解(Donoho，2006；Bioucas-dias和Figueiredo，2007)；

步骤 3 固定$\boldsymbol{\alpha}$，更新字典$\boldsymbol{D}_{\mathrm{C}}$；在这一阶段，稀疏表示系数$\boldsymbol{\alpha}_i$是已知的，式(4)可忽略等号右边的第二项，即：

$$\boldsymbol{D}_{\mathrm{C}}=\arg\min_{\boldsymbol{D}_{\mathrm{C}}}\left\|\boldsymbol{X}_{\mathrm{C}}-\boldsymbol{D}_{\mathrm{C}}\cdot\boldsymbol{\alpha}\right\|_2^2 \tag{6}$$

上式为一个二次规划问题，本文采用Lee所给出的方法求解(Lee 等，2007)；

步骤 4 返回**步骤 2**，进行迭代。

算法经过有限次迭代(本文实验中给定迭代次数为25)，便可获得式(4)的解，从而训练出所需的过完备字典对$\{\boldsymbol{D}_{\mathrm{h}},\boldsymbol{D}_{\mathrm{l}}\}$。

4 基于稀疏表示的云图超分辨率实现

下面讨论如何将训练得到的字典对$\{\boldsymbol{D}_{\mathrm{h}},\boldsymbol{D}_{\mathrm{l}}\}$应用于云图超分辨率处理。首先对待处理的低分辨率云图进行分块，对于每个低分辨率云图块y_i，考虑如下的优化问题：

$$\boldsymbol{\alpha}_i=\arg\min_{\boldsymbol{\alpha}_i}\left\|F\cdot\boldsymbol{D}_{\mathrm{l}}\cdot\boldsymbol{\alpha}_i-F\cdot\boldsymbol{y}_i\right\|_2^2+\lambda_i\left\|\boldsymbol{\alpha}_i\right\|_1 \tag{7}$$

式中，F为特征提取算子，上式右边第一项衡量重构云图与原始云图的总体相似程度，第二项是稀疏性约束。虽然求解式(7)可得到每个低分辨率云图块的表示系数$\boldsymbol{\alpha}_i$，将其作用于$\boldsymbol{D}_{\mathrm{h}}$，便可求得对应的高分辨率云图块$x_i=\boldsymbol{D}_{\mathrm{h}}\boldsymbol{\alpha}_i$，然而如果对每个云图块单独处理，则会在重构的高分辨率云图中引入块效应，为了减轻这一负面影响，本文采用一种块重叠的联合优化方案，并引入最速下降法，使得高分辨率云图满足重构约束条件，具体如下：

步骤 1 针对待处理的低分辨率云图，设计一种具有重叠像元的分块方法，本文采用使得每一云图块$\boldsymbol{y}_i$的大小为3×3，重叠度为1，即相邻块重叠一行或一列，具有3个重叠像元(如果放大2×2倍，则对应的高分辨率云图块$\boldsymbol{x}_i$的大小为6×6，重叠度为2，具有12个重叠像元；同理，如放大3×3倍，则重叠度为3)；

步骤 2 按光栅扫描的顺序对每一云图块进行处理，通过联合求解如下优化问题，得到云图块的稀疏表示系数$\boldsymbol{\alpha}_i$：

$$\boldsymbol{\alpha}_i=\arg\min_{\boldsymbol{\alpha}_i}\left\|F\cdot\boldsymbol{D}_{\mathrm{l}}\cdot\boldsymbol{\alpha}_i-F\cdot\boldsymbol{y}_i\right\|_2^2+\lambda\left\|\boldsymbol{\alpha}_i\right\|_1 \tag{8}$$

$$\boldsymbol{\alpha}_i=\arg\min_{\boldsymbol{\alpha}_i}\left\|O\cdot\boldsymbol{D}_{\mathrm{h}}\cdot\boldsymbol{\alpha}_i-\boldsymbol{R}\right\|_2^2+\beta\left\|\boldsymbol{\alpha}_i\right\|_1 \tag{9}$$

式中，$\boldsymbol{O}$为提取重叠区域的算子，$\boldsymbol{R}$为由相邻已重构的高分辨率云图块中与当前处理块重叠的像元所组成的矩阵，为简单起见，Lagrange乘子λ和β均取1，则式(8)、式(9)可写成：

$$\boldsymbol{\alpha}_i=\arg\min_{\boldsymbol{\alpha}_i}\left\|\boldsymbol{D}'\cdot\boldsymbol{\alpha}_i-\boldsymbol{y}'\right\|_2^2+\left\|\boldsymbol{\alpha}_i\right\|_1 \tag{10}$$

式中，$\boldsymbol{D}'=\begin{bmatrix}F\cdot\boldsymbol{D}_{\mathrm{l}}\\O\cdot\boldsymbol{D}_{\mathrm{h}}\end{bmatrix}$，$\boldsymbol{y}'=\begin{bmatrix}F\cdot\boldsymbol{y}\\\boldsymbol{R}\end{bmatrix}$；

步骤 3 生成对应的高分辨率云图块$\boldsymbol{x}_i=\boldsymbol{D}_{\mathrm{h}}\cdot\boldsymbol{\alpha}_i$；

步骤 4 对每一云图块都处理完成后，组成初始的高分辨率云图：$\boldsymbol{X}_0=\{\boldsymbol{x}_i\}_{i=1}^{K}$；

步骤 5 针对$\boldsymbol{X}_0$，解如下优化问题，使得最终的高分辨率云图满足重构约束条件：

$$\boldsymbol{X}=\arg\min_{\boldsymbol{X}}\left\|\boldsymbol{S}\cdot\boldsymbol{B}\cdot\boldsymbol{X}-\boldsymbol{Y}\right\|_2^2+\left\|\boldsymbol{X}-\boldsymbol{X}_0\right\|_2^2 \tag{11}$$

式中，$\boldsymbol{B}$是云图的模糊降晰算子(考虑到卫星云图的低通模糊主要由大气湍流引起，其转移函数可近似为：$B(u,v)=\exp[-c(u^2+v^2)^{5/6}]$，本文中$c$取0.00025)，$\boldsymbol{S}$为下采样算子，上式右边第一项表示了云图降晰模型，第二项描述了重构图像与理想图像的总体相似程度，对式(11)采用最速下降法求解，得到较理想的超分辨率云图$\boldsymbol{X}$。

5 数值试验

下面将通过数值实验来验证本文超分辨率算法的有效性，并与Chang提出的NE算法(邻域数目参数k取10)、基于插值放大的最近邻插值算法及双三次插值算法进行比较。实验分别从超分辨率云图的视觉效果、峰值信噪比(PSNR)及信息熵几方面来评价不同算法的性能。

训练云图取自MTSAT卫星的高分辨率通道(可见光通道)，首先选取一系列原始的可见光云图，经模糊降质并下采样后得到低分辨率云图，然后按第3节所述的方法对高、低分辨率云图分块，从而形成高、低分辨率云图块的样本对，本文共提取出10000对云图块作为训练样本，所训练出的字典$\boldsymbol{D}_{\mathrm{l}}$和$\boldsymbol{D}_{\mathrm{h}}$均包含1024个原子(此字典对可用于实现$2\times2$的超分辨率放大，如要改变放大倍数，只需重新训练合适的字典对即可)。在具体的算法实现中，需要考虑特征选择的问题，由于针对云图的超分辨率处理，低分辨率云图的高频部分比低频部分包含更多的有用信息，因此

采用Chang所采用的方法(Chang，2004)，选一阶模板[–1，0，1]和二阶模板[1，0，–2，0，1]作为式(7)、式(8)中的特征提取算子。

对训练所得的过完备字典对用于可见光及红外云图的超分辨率处理，选取MTSAT卫星2009-08-06 T 12:06的红外IR2通道和可见光通道数据作为测试云图，当时台风莫拉克已经生成，为了便于分析处理结果，从原始图像中剪切出特定的区域，剪切的原则是保证图像中台风云系相对完整。对于可见光云图，由于其本身具有较高的分辨率，首先按云图退化模型降质及下采样，生成低分辨率云图，然后进行放大，并从PSNR及信息熵两方面考察算法性能；而对于红外云图，由于其原始分辨率较低，对它直接进行超分辨率处理，以测试不同算法的实际放大效果，并仅从信息熵角度评价算法性能。图1给出了采用不同方法的可见光云图2 × 2放大的仿真结果。

从实验结果看，基于插值的算法尽管能较好地放大云图中的大尺度结构，但对小尺度的纹理信息损失严重，从局部放大的区域可以明显看出，插值运算的结果存在严重的棋盘格效应，且图像整体比较模糊；

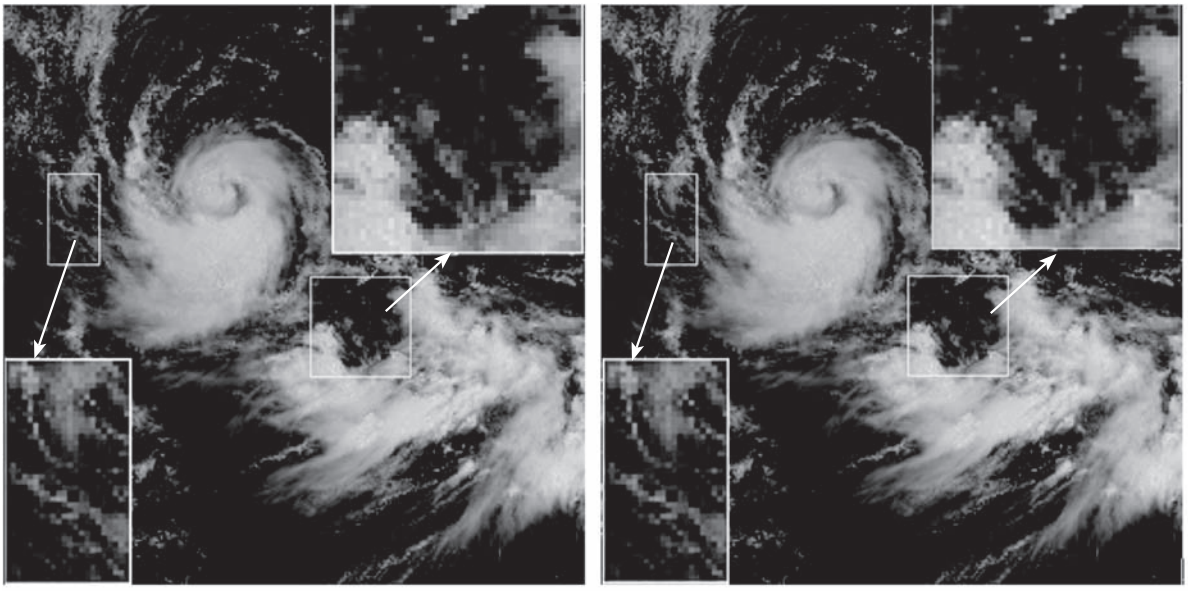

(a) 最近邻插值算法　(b) 双三次插值算法

(c) NE算法　(d) 本文算法

图1　不同方法的超分辨重建图像

NE算法与本文算法虽然均能有效地保持纹理等小尺度细节，但本文算法的重建结果更加清晰，况且NE算法重建结果的优劣取决于能否合理选取邻域数目，另一方面，NE算法的计算复杂度较高(当算法运行于Core 1.83 G CPU，1 MB RAM的笔记本电脑上时，NE算法和本文算法的平均重构时间分别为93.51 s和37.26 s)，因此相对来说本文算法更快。

为定量评价不同算法的性能，本文采用PSNR及信息熵作为客观评价指标，对于云图超分辨率而言，PSNR衡量了超分辨率结果相对于原始高分辨率云图的保真度，而信息熵度量了云图包含信息量的多少，一般来说它们的值越大，超分辨率的效果和质量越好。同时，为了测试本文算法针对其他卫星云图的可行性和有效性，本文同时选取FY/2D卫星2011-03-25 T 12∶30中国陆地区域的IR2通道和可见光通道数据进行超分辨率实验。表1分别给出了MTSAT卫星与FY/2D卫星数据的量化评价指标(对于红外云图，由于直接对其进行超分辨率处理，因此仅从信息熵角度评价算法性能)。

表1 不同算法重建结果PSNR和Entropy的比较

卫星数据	不同算法	可见光云图		红外云图(IR2)	
		PSNR	信息熵	PSNR	信息熵
MTSAT卫星	本文算法	32.6693	7.5127	—	7.2304
	NE算法	32.6704	7.2119	—	7.1291
	最近邻插值算法	27.0065	6.9364	—	7.0338
	双三次插值算法	28.4253	7.0142	—	7.0556
FY/2D卫星	本文算法	35.8905	7.2872	—	6.9230
	NE算法	35.2735	7.2145	—	6.8745
	最近邻插值算法	29.1769	7.0524	—	6.5237
	双三次插值算法	31.2348	7.0891	—	6.6381

从上表可以看出，不管对于可见光还是红外云图，本文算法在不同的评价指标上都明显优于插值放大算法，其中最近邻插值算法具有最低的PSNR和信息熵，NE算法虽然在PSNR指标上与本文算法接近，但在信息熵指标上相对较差，这也印证了NE算法所得的超分辨率结果往往过于平滑，损失了一定的细节信息；究其原因，认为气象云图多是纹理型的，局部的纹理细节比较丰富，本文所训练的过完备字典对能很好地表达云图的纹理特征，正好适合处理此类信号。

6 结 论

本文将过完备字典稀疏表示理论融入云图超分辨率处理中，通过学习获得包含高、低分辨率云图信息的过完备字典对，采用重叠分块方案，求解低分辨率云图在字典上的稀疏表示，并将表示系数用于对应的高分辨率字典，重构出高分辨率云图。实验结果表明，本文算法的重构云图在视觉效果及定量指标上均优于传统方法，这不仅说明对气象云图进行超分辨率处理是可行的和有效的，而且拓展了图像稀疏表示理论的应用范围，也为云图数据在云型分类及对流云团识别等方面的后续研究打下了良好的基础。

志 谢 感谢评审专家及宁波大学周亚训教授所提出的宝贵意见。

参考文献(References)

Bioucas-Dias J M and Figueiredo M A T. 2007. A new TwIST: two-step iterative shrinkage/thresholding algorithms for image restoration. IEEE Transactions on Image Processing, 16(12): 2992–3004

Chang H, Yeung D Y and Xiong Y M. 2004. Super-resolution through neighbor embedding. IEEE Conference on Computer Vision and Pattern Classification (CVPR), 1: 275–282

Donoho D L. 2006. For most large underdetermined systems of equations, the minimal norm near-solution approximates the sparsest near-solution. Communications on Pure and Applied Mathematics, 59(7): 907–934

Elad M and Aharon M. 2006. Image denoising via sparse and redundant representations over learned dictionaries. IEEE Transactions on Image Processing, 15(12): 3736–3745

冯鹏, 魏彪, 潘英俊, 米德伶. 2008. 基于拉普拉斯塔型变换的Contourlet变换频谱混叠特性分析. 光学学报, 28(11): 2090–2096

Georgiev C G and Kozinarova G. 2009. Usefulness of satellite water vapour imagery in forecasting strong convection: a flash-flood case study. Atmospheric Research, 93(1-3): 295–303

Lee H, Battle A, Raina R and Ng A Y. 2007. Efficient sparse coding algorithms In Advances in Neural Information Processing Systems (NIPS): 801–808

Li F, Jia X P, Fraser D and Lambert A.2010. Super resolution for remote sensing images based on a universal Hidden Markov Tree model. IEEE Transactions on Geoscience and Remote Sensing, 48(3):1270–1278

Merino M T, Nunez J. 2007. Super-resolution of remotely sensed images with variable-pixel linear reconstruction. IEEE Transactions on Geoscience and Remote Sensing, 45(5): 1446–1457

Provost J and Lesage F. 2009. The application of compressed sensing for photo-acoustic tomography. IEEE Transactions on Medical Imaging, 28(4): 585–594

Rauhut H, Schnass K and Vandergheynst P. 2008. Compressed sensing and redundant dictionaries. IEEE Transactions on Information Theory, 54(5): 2210–2219

Ricciardelli E, Romano F and Cuomo V. 2008. Physical and statistical approaches for cloud identification using Meteosat Second Generation-Spinning Enhanced Visible and Infrared Imager Data. Remote Sensing of Environment, 112(6): 2741–2760

Yang J C, Wright J, Huang T and Ma Y. 2008. Image super-resolution as sparse representation of raw image patches. IEEE Conference on Computer Vision and Pattern Classification (CVPR): 1–8